International Society for Rock Mechanics and Rock Engineering
Norwegian Group for Rock Mechanics

ISRM International Symposium
Eurock 2025 – Expanding the Underground Space
Trondheim, Norway, 16-20 June
ISBN 978-82-8208-079-8

Experimental investigation of pore collapse in Brazilian pre-salt carbonates

G.L. Righetto, R.V. Sampaio and S.A.B. Fontoura
GTEP – Group of Technology in Energy and Petroleum / PUC-Rio – Pontifical Catholic University of Rio de Janeiro, Rio de Janeiro, Brazil
righetto@puc-rio.br

C. Lima
Equinor Research and Technology Center Rio, Rio de Janeiro, Brazil

M. Naumann
Equinor ASA, Bergen, Norway

Abstract

In the oil and gas context, the fluid withdrawn within the reservoir rock causes pore pressure depletion and, consequently, an increase in the effective stress supported by the rock's solid structure. In the laboratory, one of the stress paths used to represent this scenario is hydrostatic compression, in which the rock is evenly loaded in all directions, increasing the effective mean stress (p'). Depending on the stress level, this process can lead to a significant and irreversible reduction of the pore space, known as pore collapse. In the field, some issues related to pore collapse are the reduction of hydrocarbon recovery, wellbore instability, reservoir compaction, and surface subsidence.

This work investigated well plugs from the Barra Velha Formation, which are complex lacustrine carbonates from pre-salt reservoirs at Santos Basin, Brazil. The six tested samples have porosity ranging from 12.4% to 26.3%, with permeability values between 0.02 mD and 1.4 D. Two types of configurations were employed in the tests: (i) constant pore pressure and (ii) constant confining pressure, some of them with cyclic loading stages and constant-stress periods to evaluate the time-dependent behavior.

Considering the range of porosity, pore collapse occurred at different levels of p' ranging from 36.0 to 133.1 MPa, which points towards the complexity of the micromechanics associated with this phenomenon in porous carbonate rocks. The bulk compressibilities of the specimens were obtained previous to the tests, which allowed for the calculation of the Biot's coefficient (α). Additionally, the evaluation was supported by the acquisition of ultrasonic waves transit time during the tests and X-ray μCT images of the samples before and after testing. This study contributes to understanding the mechanical behavior of carbonate rocks in the Brazilian pre-salt reservoirs, which are currently the source of approximately 80% of the country's total hydrocarbon production.

Keywords

Pore collapse, Brazilian pre-salt carbonates, Barra Velha Formation, Experimental investigation.

ISRM

NBG

1 Introduction

The modification of the rock's pore space, either by compaction or dilation, is closely related to the loading path to which the rock is subjected (Wong et al. 1997; Zhu and Wong 1997; Wong and Baud 2012), as shown in Fig. 1. At the beginning of the loading, the nonlinear behavior is associated with the closure of pre-existing microcracks and pores with high aspect ratio, up to a stress level above where elastic deformation takes place. After that, the onset of the nonlinear behavior will depend on the loading path. For a hydrostatic loading, the inflection point occurs at a critical stress accompanied by a significant and permanent reduction in porosity. For nonhydrostatic loading types, when differential stress is applied, the transition between dilation and contraction is related to the value of confining pressure and, consequently, the mean effective stress (p'). At low confinements, the shear-induced dilation is typical of brittle failure, meanwhile, the ductile type of failure at higher values of confinement leads to a shear-enhanced compaction of the specimen.

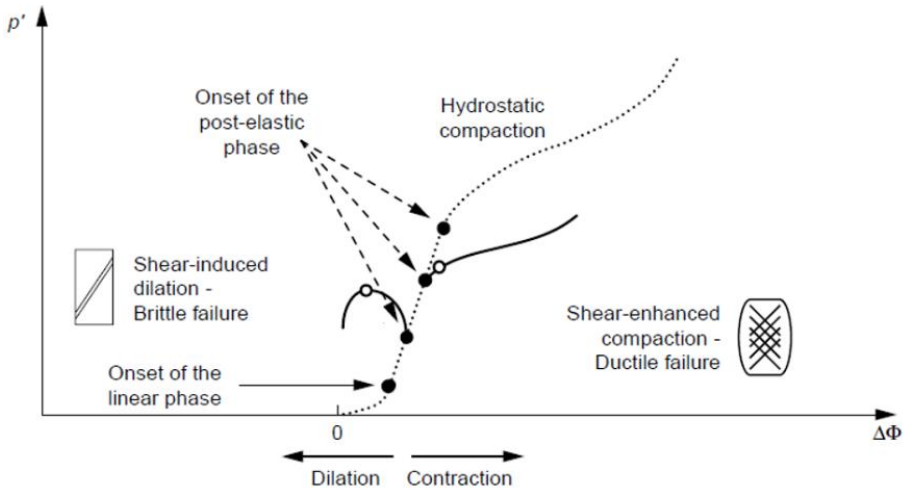

Fig. 1 Evolution of rock's porosity (ϕ) with effective mean stress (p') during triaxial tests (solid lines) at low (brittle failure) and high (ductile failure) confining pressure, and hydrostatic tests (dotted line). Adapted from Bemer et al. (2004).

In the oil and gas context, the fluid withdrawn within the reservoir causes a pore pressure depletion and an increase in the mean effective stress supported by the rock's solid structure. In response to this process, the volumetric compaction may lead to inelastic deformation and an irreversible reduction of the rock's porosity, known as pore collapse (Addis 1987; Smits et al. 1988). In the field, the main issues related to the collapse of the pore space include reduced hydrocarbon recovery (due to decreased permeability), sand production, wellbore instability, casing deformation, induced seismicity, reservoir compaction, and surface subsidence (Wiborg and Jewhurst 1986; Zaman et al. 1994; Boutéca et al. 1996; Segall 1989; Fredrich et al. 2000; Wong et al. 2004).

Even though clastic rocks and carbonates present very similar characteristics from the phenomenological point of view, the micromechanics associated with the compaction behavior are quite different (Zhu et al. 2010). In clastic rocks, such as sandstones, the inelastic compaction occurs mostly due to grain crushing, from the stress concentration at grain contacts, according to laboratory investigation, and it can be analyzed by Hertzian fracture mechanics models (Zhang et al. 1990; Menéndez et al. 1996; Wu et al. 2000; Mair et al. 2002; Wong and Baud 2012). On the other hand, the microscopic observation on carbonate rocks pointed out that compaction starts from the stress concentration at the surface of a pore, emanating a ring of localized damage around it (Fig. 2). Wong and Baud (2012) mentioned that in low-porosity limestones the behavior could be interpreted as the collapse of spherical pores caused by crystal plasticity processes such as dislocation slip and deformation twinning, as described by the Curran and Carroll (1979) model. However, studies with carbonates with higher porosity (Vajdova et al. 2004; Zhu et al. 2010) have shown that the compaction in this type of rock is far more complicated than the previous model could predict. According to the authors, the collapse in porous carbonates seems to initiate in the larger pores, and the processes of cataclasis and microcracking dominate the deformation around the collapsed pore, rather than crystal plasticity. This type of compaction is called "cataclastic pore collapse" and the pore space is treated as a dual porosity medium (micro and macro pores), rather than a single entity, considering the bimodal pore size distribution observed in these carbonates. Despite the challenges of attempting to model the

compaction behavior in such complex rocks, the compilation presented by Zhu et al. (2010) shows an overall trend of a decreasing onset of collapse with increasing porosity.

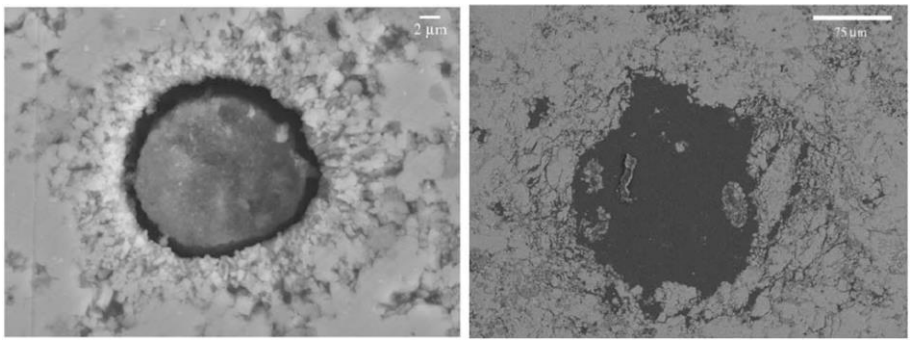

(a) (b)

Fig. 2 Backscattered SEM images of deformed samples of Tavel limestone (ϕ = 13.6%) at (a) hydrostatic test and (b) triaxial test at 150 MPa of confining pressure showing the cataclastic pore collapse with a halo of massive damage around large pores. Source: Zhu et al. (2010).

The experimental investigation allows the assessment of the stress states responsible for the onset of pore collapse, providing the necessary data to calibrate constitutive models that encompass both brittle and ductile types of failure, either by an extension of the shear strength envelope with an elliptical cap or by non-linear models, such as the well-known Cam-Clay (Schofield and Wroth 1968; DiMaggio and Sandler 1971; Sandler et al. 1976; Chen 1980; Chen 1982; Chen and Mizuno 1990; Coelho et al. 2006). In these types of constitutive models, the hydrostatic compression data, presented in this paper, is fundamental to the definition of the envelope, as shown in Fig. 3. The propagation of ultrasonic waves during the hydrostatic test is also very useful in identifying the pore collapse since the wave's velocity shows a clear deceleration at this point.

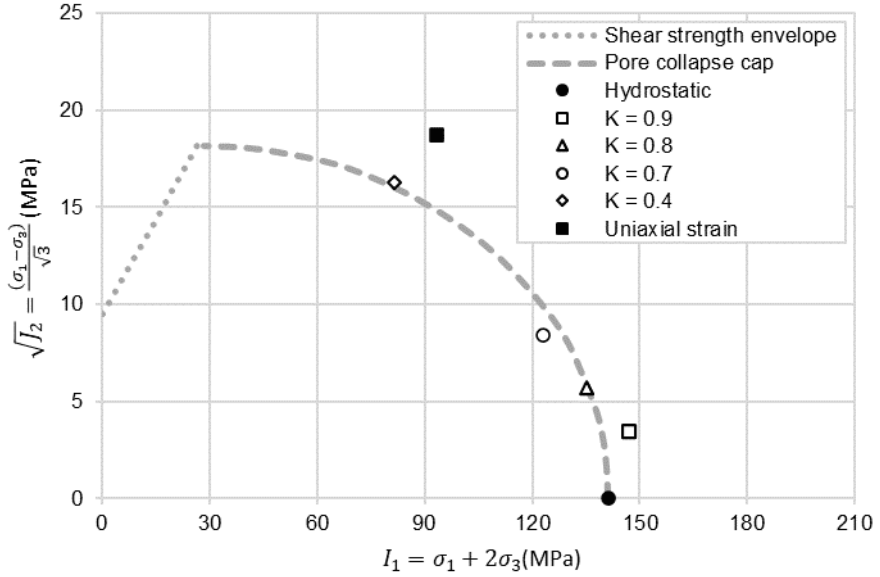

Fig. 3 Shear envelope and pore collapse (elliptical cap) in terms of first and second stress invariants obtained by Coelho et al. (2006) for a Brazilian limestone with porosity around 20 and 30% from an oil reservoir at Campos Basin.

2 Studied rock

The six samples presented in this paper are plugs from three wells (A, B, and C) located in Santos Basin, Southeast Brazil. The samples were obtained from oil and gas reservoirs in the pre-salt region and they are lacustrine carbonates of the Barra Velha Formation. These carbonates are quite challenging due to their complex textures and pore spaces, as well as a high level of heterogeneity resulting from a combination of depositional characteristics and diagenetic processes. This complexity leads to a diversity of lithologies and petrophysical properties as observed in the tested plugs (Table 1). The details of the geology and petrophysics of these samples are beyond the scope of the present work and can be found in Sampaio et al. (2023). With approximately 80% of the Brazilian hydrocarbons production coming from the pre-salt reservoirs (ANP 2024), several authors have been studying this type of rock, mostly their geology and petrophysics (Rezende and Pope 2015; Herlinger

et al. 2017; Vieira de Luca et al. 2017; Lima and De Ros 2019; Gomes et al 2020; Lima et al. 2020; Sartorato et al. 2020; Wright and Barnett 2020; Basso et al. 2021; Carvalho et al. 2022; Wright 2022; de Ros and Oliveira 2023; Ruiz and Batezelli 2024). However, collecting samples from such great depths remains a challenging and costly task and there is still a lack of experimentally obtained mechanical parameters for these carbonates. This paper aims to supplement the findings by Sampaio et al. (2024) regarding the strength characterization of samples from the same wells studied herein.

Table 1. Samples used in the experimental program. Porosity (ϕ), and permeability (k) were obtained by gas (He/N) permeameter-porosimeter at 3.5 MPa of confining pressure.

Sample	Lithology	ϕ (%)	k (mD)
A1	Spherulitc shrubstone	16.0	51.7
A2	Spherulitc shrubstone	16.3	17.5
B1	Shrubby framestone	12.4	0.02
B2	Shrubby framestone	16.9	25.2
B3	Spherulitic packstone/grainstone	26.3	1436.3
C1	Packstone	14.2	18.9

3 Experimental program

The experimental program was based on hydrostatic compression tests performed using a GCTS RTX-3000 equipment, with LVDT (Linear Variable Differential Transformers) sensors measuring the axial and radial displacements of the samples. The transit time of compressional and shear ultrasonic waves (200 kHz) was monitored throughout the entire test using piezocrystals installed in the loading caps of the triaxial equipment. The plugs were prepared according to ASTM (2019) standards and saturated with distilled water, except for sample B1 (see Table 1), which was tested in dry conditions due to its very low permeability. The cylindrical plugs from wells A and C were 1.5 inches in diameter, with a height/diameter ratio (H/D) between 2 and 3. The plugs from well B were smaller, 1 inch in diameter, and around 1.8 of H/D. Despite the lower H/D, they were included in the experimental program because of their importance in the context of pre-salt carbonates.

Considering the definition of Terzaghi's effective mean stress (p') described in Eq. 1 (see Terzaghi 1943), two types of configurations (Fig. 4) were employed in the hydrostatic tests to load the sample: (I) increasing the confining pressure at a constant value of pore pressure and (II) decreasing the pore pressure at a constant value of confining pressure. In the type I configuration, the maximum confining pressure should not exceed the equipment's safe operational limit of 140 MPa, meanwhile, the limit for type II was associated with the full unloading of the 90.3 MPa of pore pressure, which was determined based on field observations and applied to all tests with saturated samples. The axial differential stress was kept constant at 2.5 MPa in all tests and a loading rate of 1MPa/min was applied to both confining and pore pressures. Transducers monitored the inlet and outlet pore pressure to guarantee the even distribution inside the specimen and the drained condition of the tests. In some cases, the loading was performed in two cycles to evaluate elastic parameters and permanent deformation. Stages of holding constant stresses were also added to assess the time-dependent behavior of the rock.

$$p' = p - p_p = \frac{(\sigma_1 + 2\sigma_3)}{3} - p_p = \frac{(\sigma_3 + \sigma_d + 2\sigma_3)}{3} - p_p = \left(\frac{\sigma_d}{3} + \sigma_3\right) - p_p \quad (1)$$

Where p' Terzaghi's effective mean stress
p Total mean stress
p_p Pore pressure
σ_1 Maximum principal stress (axial stress)
σ_3 Minimum principal stress (confining pressure)
σ_d Axial differential stress

Two steps were included in the configuration of the tests, once the desired stresses were achieved, to calculate the bulk modulus and Biot's coefficient following the ISRM suggested methods (Dudley et al. 2016). Loading cycles of 2 MPa were applied to the confining and pore pressures and the parameters were calculated by Eq. 2 to 5.

$$C_{bc} = -\frac{1}{V_B}\left(\frac{\partial V_B}{\partial p}\right)_{p_p = const} \quad (2)$$

$$C_{bp} = \frac{1}{V_B}\left(\frac{\partial V_B}{\partial p_p}\right)_{p = const} \quad (3)$$

$$K_{bc} = \frac{1}{C_{bc}};\ K_{bp} = \frac{1}{C_{bp}} \quad (4)$$

$$\alpha = \frac{K_{bc}}{K_{bp}} \quad (5)$$

Where C_{bc} Bulk compressibility at constant pore pressure
C_{bp} Bulk compressibility at constant mean stress
V_B Bulk volume
K_{bc} Bulk modulus at constant pore pressure
K_{bp} Bulk modulus at constant mean stress
α Biot's coefficient

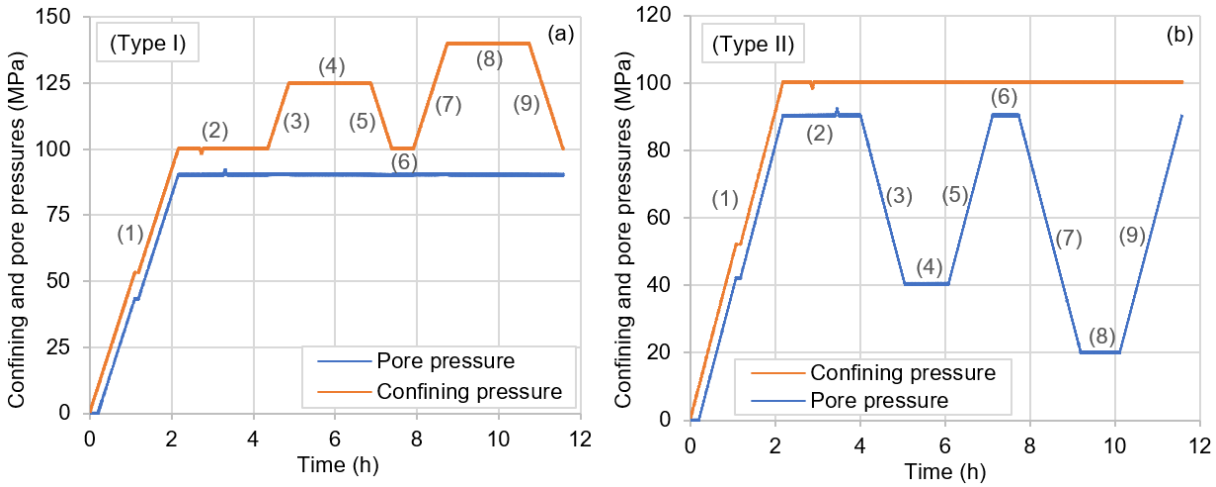

Fig. 4 Example of configuration types I and II. Phases of the test: (1) achieving the desired initial stresses; (2) cycles to obtain the poroelastic properties; (3) and (7) loading/reloading of p'; (5) and (9) unloading of p'; (4), (6) and (8) constant stresses to evaluate time-dependent behavior.

4 Results

The results of the hydrostatic tests are summarized in Table 2. Fig. 5 shows examples obtained with samples A2 and B3, using types I and II of configurations, respectively. The loading and reloading stages (see phases 3 and 7 of Fig. 4) resulted in slightly different bulk modulus values for both samples, with K_7 higher than K_3 due to the permanent compaction already achieved in the first loading cycle, increasing the rock stiffness. The irrecoverable strain after the first cycle is a combination of the initial non-linear phase (closing of pre-existing microcracks and pores with a high aspect ratio), and the creep deformation during the period of constant stresses (Fig. 5c, d). The time-dependent strain responses observed during the tests suggest that creep behavior can be important for selecting proper constitutive models for this type of rock, and further investigations are needed.

The ultrasonic wave velocity behaved as anticipated (Fig. 5a, b), exhibiting an increment of p' up to the point where the onset of pore collapse occurred. After this point, a velocity deceleration can be observed, even with the increase in p'. Another indication of the collapse of the rock's pore space is the drop in porosity (Fig. 5e, f) calculated using the deformation readings (see Dudley et al. 2016). Reductions of 1% and 0.3% were obtained for samples B3 and A2, respectively.

Table 2. Results of the hydrostatic tests. K_3 and K_7 are the bulk modules obtained in the loading and reloading stages, respectively. Samples are ordered by porosity.

Sample	ϕ (%)	k (mD)	K_{bc} (GPa)	K_{bp} (GPa)	$\alpha = K_{bc}/K_{bp}$	K_3 (GPa)	K_7 (GPa)	$p'_{collapse}$ (MPa)
B1	12.4	0.02	-	-	-	15.2	25.6	133.1
C1	14.2	18.9	15.6	27.0	0.58	48.4	48.3	86.0
A1	16.0	51.7	14.5	16.4	0.88	11.5	-	36.0
A2	16.3	17.5	15.2	18.5	0.82	8.6	12.1	41.0
B2	16.9	25.2	20.0	24.4	0.82	38.1	-	76.5
B3	26.3	1436.3	5.6	10.3	0.54	9.0	13.4	63.4

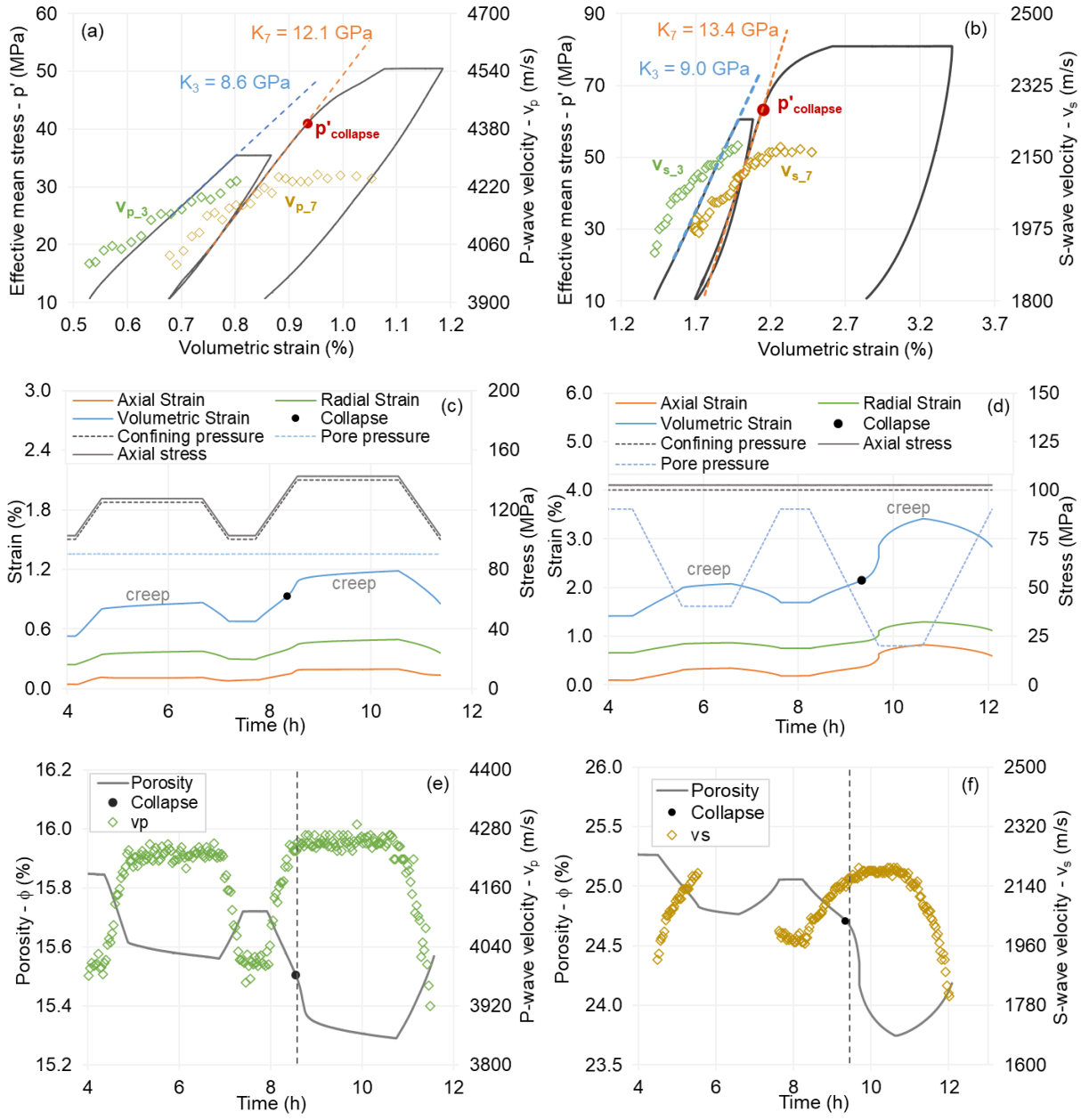

Fig. 5 Examples of stress-strain curves obtained with samples (a) A2 and (b) B3; evolution of strains with time (c, d) for the same samples, highlighting the creep behavior during constant-stress periods; variations in porosity and velocity of ultrasonics waves (e, f) throughout the tests (some of the ultrasonics data were lost for sample B3 due to technical issues).

Digital images were obtained using X-ray microtomography at 38µm of resolution, and the pore space models before and after the hydrostatic tests can be compared (Fig. 6). The reduction in porosity aligns with trends observed in other analyses, however, the values derived from this imaging technique are significantly lower than laboratory measurements, due to the limitation of the image resolution and the difficulty in capturing the smaller pores.

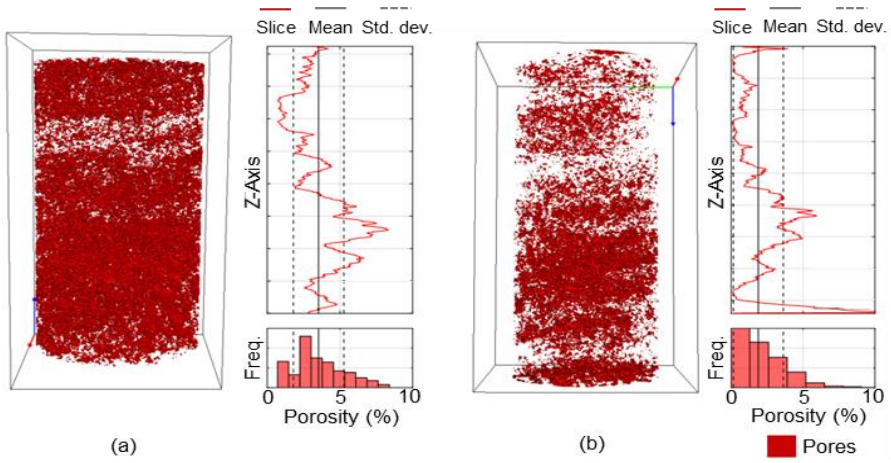

Fig. 6 Digital images from X-ray microtomography of sample A2 (a) pre and (b) post-test showing the reduction of the pore space (in red).

In addition to the fact that these samples come from different fields in Santos Basin and have distinct lithologies (see Table 1), they present some variations regarding pore space. Analysing Table 2, it is clear that porosity is not the only factor influencing the onset of collapse ($p'_{collapse}$). For example, when comparing samples A1 and B3, one could anticipate that higher porosity would lead to lower $p'_{collapse}$. However, this was not the case. The first indication that these samples would not easily fit into the same group was the significant variation in permeability. Fig. 7 illustrates the differences in the pore space of the aforementioned samples A1 and B3. Mercury intrusion porosimetry tests were conducted on rock fragments (obtained after drilling the plugs) from depths near these samples, providing insights into their pore size distribution. The samples from well A exhibited approximately 40% of their pores in the range of 10 to 100 µm, while in the same range, the tests with well B samples showed only around 10% of their pores. The rock fragments from well A displayed multiple peaks in the incremental curves, which is characteristic of a highly heterogeneous pore size distribution known as multimodal. In contrast, the pore space of the samples from well B was more homogeneous, with a concentration around the 1.0 µm size. Additionally, the median pore size diameter was 3.1 µm for well A, compared to 1.4 µm for well B.

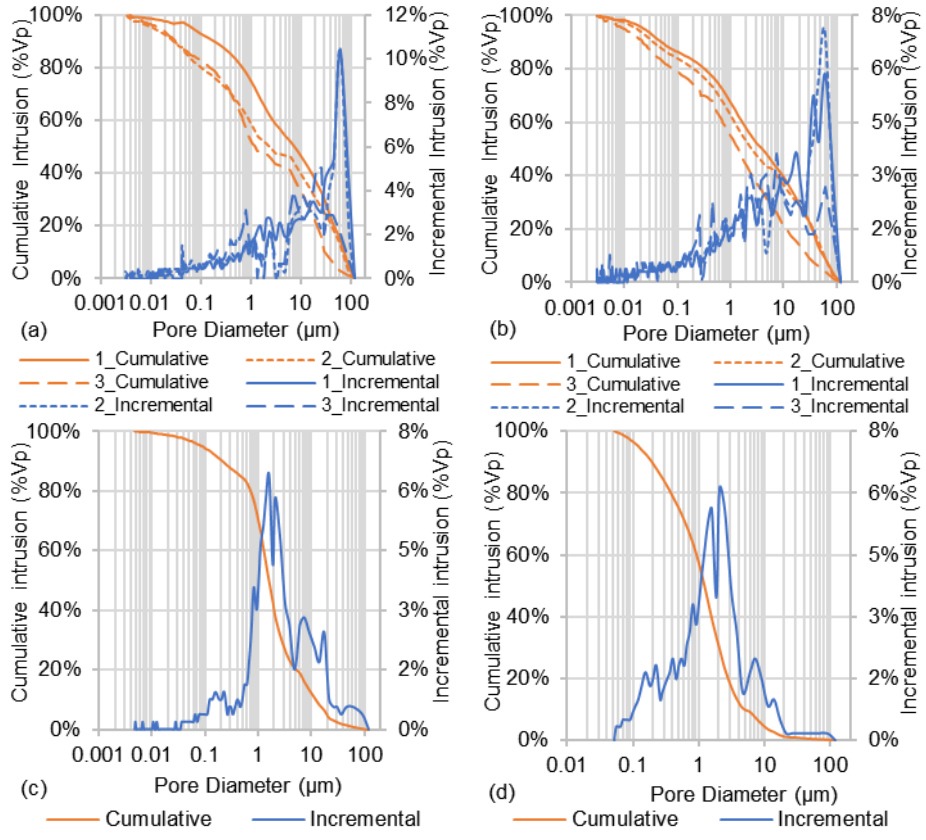

Fig. 7 Pore size distribution curves obtained with fragments from wells (a, b) A and (c, d) B at depths close to samples A1, A2, B2, and B3. The tests were performed using mercury intrusion porosimetry.

The different microstructures of the samples, associated with the different lithologies, also played an important role in the poroelastic properties, such as the bulk modulus, as presented in Table 2. The higher the porosity, the lower the bulk modulus (K_{bc}), except for sample B2. Based on the Biot's coefficients, it is possible to define two main groups: $0.82 < \alpha < 0.88$ and $0.54 < \alpha < 0.58$. The samples related to the former have shrubs/spherulites as the main component in the framework (Sampaio et al 2023). On the other hand, the latter were classified as packstone (grain-supported muddy rock), i.e., with a different depositional texture, according to Dunham's classification (Dunham 1962).

These observations are consistent with the findings of Vajdova et al. (2004) and Zhu et al. (2010) regarding the micromechanics of cataclastic pore collapse in porous carbonate rocks. They noted that collapse is more likely to initiate around larger pores, which suggests that porosity should not be considered a single, uniform property. This could explain the low collapse stress observed in sample A1, which contains larger pores, even though its total connected porosity is lower compared to sample B3. Further testing would be required to assess the applicability of the Zhu et al. (2010) micromechanical model for pore collapse in carbonates from the Barra Velha Formation. Yet, the feasibility of conducting such additional tests typically faces challenges due to the limited availability of core samples and the associated constraints of time and cost.

Considering a wider context, the pore collapse pressure of calcite-rich porous rocks may have a reasonable correlation with porosity. Based on the data compilation presented by Wong and Baud (2012), the Barra Velha Formation results could be contextualized (Fig. 8). Although the carbonate rocks exhibit different lithologies, it was possible to establish a satisfactory power law correlation. It is important to note that this correlation should only be used as a preliminary estimate, particularly for complex rocks such as the carbonates from the Brazilian pre-salt. While this correlation may be useful when no specimens are available for experimental testing, it should not replace the actual execution of tests to determine the onset pressure of pore collapse.

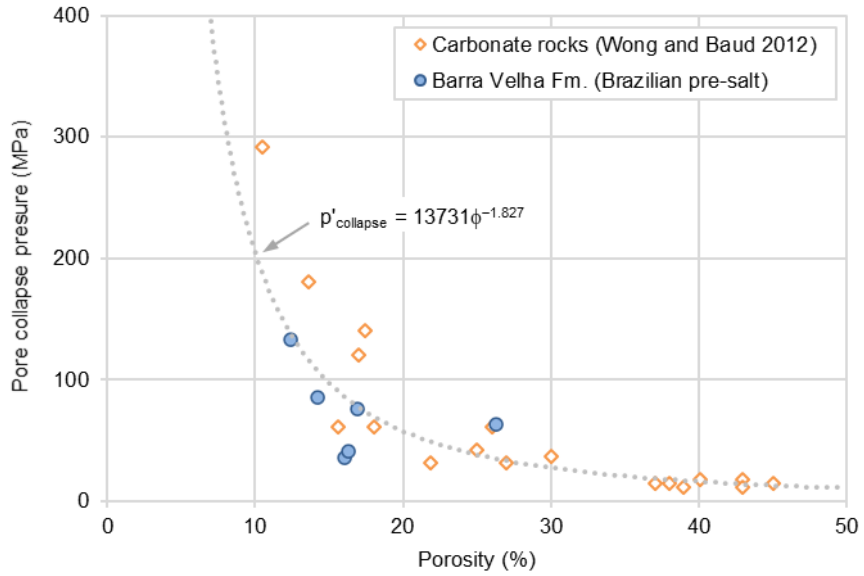

Fig. 8 Correlation between pore collapse stress and porosity for carbonate rocks.

5 Conclusions

Despite the limited number of samples from the Brazilian pre-salt region, the findings presented here enhance the understanding of the mechanical behavior of these complex rocks. The hydrostatic tests conducted on six samples from the Barra Velha Formation successfully determined the stress level at which pore collapse begins. This is a crucial parameter for calibrating constitutive models that incorporate the compaction cap. Despite the complex pore space of carbonate rocks, it was possible to define a correlation between the pore collapse pressure ($p'_{collapse}$) and porosity, gathering data from the literature and the results presented herein. Additionally, the tests provided important poroelastic properties of the rock, including bulk compressibility and Biot's coefficient. The results also emphasize time-dependent characteristics. Therefore, a more detailed experimental program is being planned to further characterize them.

References

Addis MA (1987) Material Metastability in Weakly Cemented Sedimentary Rocks. Memoir of the Geological Society of China. 495-512.

ANP - Brazilian National Petroleum Agency, Natural Gas and Biofuels. (2024). Bulletin of Oil and Natural Gas Production (In Portuguese).

ASTM (2019) D4543: Standard Practices for Preparing Rock Core as Cylindrical Test Specimens and Verifying Conformance to Dimensional and Shape Tolerances. ASTM International, USA. DOI: 10.1520/D4543-19

Basso M, Belila AMP, Chinelatto GF, Souza JPP, Vidal AC (2021) Sedimentology and petrophysical analysis of pre-salt lacustrine carbonate reservoir from the Santos Basin, southeast Brazil. Int J Earth Sci Geol Rundsch (110): 2573–2595.

Bemer E, Vincké O, Longuemare P (2004) Oil & Gas Science and Technology - Rev. IFP (59, 4): 405-426. DOI: 10.2516/ogst:2004028

Boutéca M, Sarda JP, Schneider F (1996) Subsidence induced by the production of fluids. Rev. Inst. Fr. Pet. (51): 349– 379.

Carvalho AAM, Hamon Y, de Souza Jr. OG, Carramal NG, Collard N (2022) Facies and diagenesis distribution in an Aptian pre-salt carbonate reservoir of the Santos Basin, offshore Brazil: A comprehensive quantitative approach. Marine and Petroleum Geology (141).

Chen WF (1980) Plasticity in soil mechanics and landslides. Journal of the Engineering Mechanics Division, ASCE, 106(BM3).

Chen WF (1982) Plasticity in reinforced concrete. McGraw-Hill, New York.

Chen WF, Mizuno E (1990) Nonlinear analysis in soil mechanics – theory and implementation for structural engineers. Elsevier Science Publisher, Amsterdam.

Coelho LC, Soares AC, Ebecken NFF, Alves JLD, Landau L (2006) Modelling mechanical behaviour of limestone under reservoir conditions. International Journal for Numerical and Analytical Methods in Geomechanics (30): 1477-1500.

Curran JH, Carroll MM (1979) Shear stress enhancement of void compaction. J. Geophys. Res. (84): 1105-1112.

De Ros LF, Oliveira DM (2023). An Operational Classification System for the South Atlantic Pre-Salt Rocks. Journal of Sedimentary Research, v. 93, 693-704.

DiMaggio FL, Sandler IS (1971) Material model for granular soils. Journal of the Engineering Mechanics Division, American Society of Civil Engineers (97, EM3): 935-949.

Dudley JW, Brignoli M, Crawford BR, Ewy RT, Love DK, McLennan JD, Ramos GG, Shafer JL, Sharf-Aldin MH, Siebrits E, Boyer J, Chertov MA (2016) ISRM Suggested Method for Uniaxial-Strain Compressibility Testing for Reservoir Geomechanics. Rock Mechanics and Rock Engineering. (49): 4153-4178.

Dunham RJ (1962) Classification of carbonate Rocks according to depositional texture. In: Ham, W. E. (ed.), Classification of carbonate Rocks: American Association of Petroleum Geologists Memoir. P: 108-121.

Fredrich JT, Arguello JG, Deitrick GL, de Rouffignac EP (2000) Geomechanical modeling of reservoir compaction, surface subsidence, and casing damage at the Belridge diatomite field. SPE Reservoir Eval. Eng. (3): 348– 359.

Gomes JP, Bunevich RB, Tedeschi LR, Tucker ME, Whitaker FF (2020) Facies classification and patterns of lacustrine carbonate deposition of the Barra Velha Formation, Santos Basin, Brazilian Pre-salt. Marine and Petroleum Geology (113):104176.

Herlinger R, Zambonato EE, Ros LF (2017) Influence of diagenesis on the quality of Lower Cretaceous Pre-salt lacustrine carbonate reservoirs from Northern Campos Basin, offshore Brazil. Journal of Sedimentary Research (87): 1285-1313.

Lima BE, De Ros LF (2019) Deposition, diagenetic and hydrothermal processes in the Aptian Pre-Salt lacustrine carbonate reservoirs of the northern Campos Basin, offshore Brazil. Sediment. Geol. (383): 55–81.

Lima BE, Tedeschi LR, Pestilho ALS, Santos RV, Vasquez JC, Guzzo JVP, De Ros LF (2020) Deep-burial hydrothermal alteration of the Pre-Salt carbonate reservoirs from northern Campos Basin, offshore Brazil: evidence from petrography, fluid inclusions, Sr, C and O isotopes. Mar. Petrol. Geol. (113)

Mair K, Elphick SC, Main IG (2002) Influence of confining pressure on the mechanical and structural evolution of laboratory deformation band. Geophys. Res. Lett. (29, 10). DOI: 10.1029/2001GL013964.

Menéndez B, Zhu W, Wong T-F (1996) Micromechanics of brittle faulting and cataclastic flow in Berea sandstone. J. Struct. Geol. (18): 1– 16. DOI:10.1016/0191-8141(95)00076-P.

Rezende MF, Pope MC (2015) Importance of depositional texture in pore characterization of subsalt microbialite carbonates, offshore Brazil. In: Microbial Carbonates in Space and Time: Implications for Global Exploration and Production. (Ed. by D.W.J. Bosence; K.A. Gibbons; D.P. Le Heron; W.A. Morgan; T. Pritchard; B.A. Vining). Geological Society, London, Special Publications (418):193-207.

Ruiz MLC, Batezelli A (2024) Correlation between geomechanical and sedimentary facies and their implications for flow unit definition in the pre-salt carbonate reservoir, Brazil. Journal of South American Earth Sciences (141, 104958).

Sampaio RV, Righetto GL, Fontoura SAB, Lima C, Naumann M (2024). Strength characterization and empirical correlations for carbonate rocks from the Brazilian pre-salt reservoirs. In 58th US Rock Mechanics/Geomechanics Symposium.

Sampaio RV, Righetto GL, Gomes RGS, Fernandes LFL, Fontoura SAB, Guimarães VLO, Bueno JF, Honório, BCZ, Lima C, Naumann M, Zhou C (2023). Some petrophysical characteristics of a Brazilian Pre-salt cabonate. In 57th US Rock Mechanics/Geomechanics Symposium.

Sandler IS, DiMaggio FL, Baladi GY (1976) Generalized cap models for geological materials. Journal of the Geotechnical Engineering Division (102): 683-699.

Sartorato ACN, Tonietto SN, Pereira E (2020) Silicification and dissolution features in the brazilian Pre-salt Barra Velha formation: impacts in the reservoir quality and insights for 3D geological modeling. In: Rio Oil & Gas Expo and Conference.

Schofield A, Wroth P (1968) Critical State Soil Mechanics. McGraw-Hill, London.

Segall P (1989) Earthquakes triggered by fluid extraction. Geology. (17): 942–946.

Smits RMM, de Waal JA, van Kooten JFC (1988) Prediction of Abrupt Reservoir Compaction and Surface Subsidence Caused by Pore Collapse in Carbonates. SPE Formation Evaluation.

Terzaghi K (1943) Theoretical Soil Mechanic. Wiley. New York.

Vajdova V, Baud P, Wong T-F (2004) Compaction, dilatancy and failure in porous carbonate rocks. J. Geophys. Res. (109, B05204). DOI:10.1029/2003JB002508.

Vieira de Luca PH, Matias H, Carballo J, Sineva D, Pimentel GA, Tritlla J, Esteban M, Loma R, Alonso JLA, Jiménez RP, Pontet M, Martinez PB, Vega V (2017) Breaking barriers and paradigms in presalt exploration: the Pão de Açúcar discovery (offshore Brazil). In: Merrill, R.K., Sternbach, C.A. (Eds.), Giant Fields of the Decade 2000–2010 (113): 177-194.

Wiborg R, Jewhurst J (1986) Ekofisk subsidence – detailed and solutions assessed. Oil & Gas Journal. 47-51.

Wong T, David C, Menéndez B (2004) Mechanical compaction. Mechanics of Fluid-Saturated Rocks. 55–114. Elsevier Acad. Amsterdam.

Wong T, David C, Zhu W (1997) The transition from brittle faulting to cataclastic flow in porous sandstones: Mechanical deformation. J. Geophys. Res. (102): 3009–3025. DOI:10.1029/96JB03281.

Wong T-F, Baud P (2012) The brittle-ductile transition in porous rock: a review. Journal of Structural Geology. (44): 25-53.

Wright VP (2022) The mantle, CO2 and the giant Aptian chemogenic lacustrine carbonate factory of the South Atlantic: some carbonates are made, not born. Sedimentology (69): 47–73.

Wright VP, Barnett AJ (2020) The textural evolution and ghost matrices of the Cretaceous Barra Velha Formation carbonates from the Santos Basin, offshore Brazil. Facies (66, 7).

Wu XY, Baud P, Wong T-F. (2000) Micromechanics of compressive failure and spatial evolution of anisotropic damage in Darley Dale sandstone. Int. J. Rock Mech. Min. Sci. (37): 143-160.

Zaman M, Roegiers JC, Abdulraheem A, Azeemuddin M (1994) Pore collapse in weakly cemented and porous rocks. Journal of Energy Resources Technology. (116): 97-103.

Zhang J, Wong T, Davis DM (1990) Micromechanics of pressure induced grain crushing in porous rocks, J. Geophys. Res. (95): 341–352. DOI:10.1029/JB095iB01p00341.

Zhu W, Baud P, Wong T (2010) Micromechanics of cataclastic pore collapse in limestone. J. Geophys. Res. (115, B04405). DOI:10.1029/2009JB006610.

Zhu W, Wong TF (1997) The Transition from Brittle to Cataclastic Flow: Permeability Evolution. Journal of Geophysical Research (102, B2): 3027-3041.